In vitro determination of contact areas in the normal elbow joint of dogs

Chris A. Preston, BVSc; Kurt S. Schulz, DVM, MS; Philip H. Kass, DVM, PhD

Objective—To evaluate areas of articular contact of the proximal portions of the radius and ulna in normal elbow joints of dogs and the effects of axial load on size and location of these areas.

Sample Population—Forelimbs obtained from cadavers of 5 adult mixed-breed dogs.

Procedure—After forelimbs were removed, liquid-phase polymethyl methacrylate was applied to articular surfaces of the elbow joint, and limbs were axially loaded. Articular regions void of casting material were stained with water-soluble paint. Relative articular contact areas were determined by computer-assisted image analyses of stained specimens. Repeatability of the technique was evaluated by analyses of casts from bilateral forelimbs of 1 cadaver. Incremental axial loads were applied to left forelimbs from 4 cadavers to determine effects of load on articular contact.

Results—Specific areas of articular contact were identified on the radius, the craniolateral aspect of the anconeus, and the medial coronoid process. The medial coronoid and radial contact areas were continuous across the radioulnar articulation. There was no articular contact of the medial aspect of the anconeus with the central trochlear notch. Coefficients of variation of contact areas between repeated tests and between contralateral limbs was < 20%. Significant overall effects of axial load on contact area or location were not identified.

Conclusions—Three distinct contact areas were evident in the elbow joint of dogs. Two ulnar contact areas were detected, suggesting there may be physiologic incongruity of the humeroulnar joint. There was no evidence of surface incongruity between the medial edge of the radial head and the lateral edge of the medial coronoid process. (*Am J Vet Res* 2000;61: 1315–1321)

Determination of contact areas in diarthodial joints is necessary for understanding the state of stress within articular cartilage layers and supporting bony structures.[1] This information provides a baseline for subsequent studies of various pathologic conditions and the effects of surgical procedures, contributes to our understanding of the pathophysiologic characteristics of osteoarthritis, guides the design of prosthetic joint components, and aids in assessment of mechanical factors in aseptic loosening of joint components.[2-6] Surface incongruency, osteochondral injury, and ligamentous insufficiency alter contact areas and affect load transmission in joints. It is necessary to identify joint contact characteristics from defined pathologic conditions and objectively assess the effects of corrective osteotomies to appropriately treat altered joint surface mechanics.[1,5,7]

Diarthrodial articulations transmit forces across cartilage surfaces that are in direct contact. Normal joint surfaces are not sufficiently congruent to permit uniform load bearing over the entire surface.[8,9] Under functional loading conditions, pressure gradients exist at the cartilage surface.[5,8] Joints with a high degree of inherent congruency, such as the elbow and hock, have articulating surfaces of similar geometry and consequently have a high percentage of articular cartilage in contact throughout the normal range of motion.[8] Conversely, highly incongruous joints, such as the stifle, have articulating surfaces with dissimilar geometry, which results in a small percentage of cartilage contact.[8] Studies in human cadavers have revealed reproducible and distinct contact patterns in joints for normal specimens of individual articulations, which have been referred to as contact signatures.[5]

Compressive, as well as shear and rotational, forces are transmitted across cartilage contact areas. These forces are determined by ground reaction forces, which are typically transmitted axially, and those developed by active myotendinous units, which span joints and create moments and compressive forces. The magnitude of these forces, combined with size and topography of contact areas, determines local contact pressure across cartilage interfaces. Under fixed loading conditions, larger overall contact areas allow more distribution of forces than smaller contact areas, resulting in lower peak pressures. Excessive local pressures have been linked to chondrocyte death, damage to cartilage matrix, and initiation of osteoarthritis.[1,3,4,10-14]

Numerous studies of orthopedic biomechanics have assessed the influence of loading conditions and joint angle on contact areas in normal diarthodial joints of human cadavers.[4,5,12,13] These studies revealed significant differences in contact areas and distribution of these areas under different loading conditions.[2,4-6,12,13] In many joints in humans, size of the contact area increases with increasing load to allow continuous stress distribution and minimization of local contact pressure.[5,9]

The purposes of the study reported here were to evaluate the repeatability of **polymethyl methacrylate (PMMA)** joint casting for the determination of contact areas in the elbow joint in dogs (phase I) and to examine effects of axial load on contact area size and distri-

Received May 21, 1999.
Accepted Aug 23, 1999.
From the J.D. Wheat Veterinary Orthopedic Research Laboratory, School of Veterinary Medicine, University of California, Davis, CA 95616.
Supported by grants from the Center for Companion Animal Health and the Veterinary Medical Teaching Hospital, University of California, Davis, CA 95616.
Address correspondence to Dr. Schulz, Department of Surgical and Radiological Sciences, School of Veterinary Medicine, University of California, Davis, CA 95616.

bution in a canine forelimb model that mimicked the angle and maximum vertical peak load during a trot. Our hypothesis was that physiologic concave incongruity exists in normal elbow joints and that size and distribution of areas of contact depend on the magnitude of axial compressive load.[9,15,16]

Materials and Methods

Specimens—Forelimbs were obtained from 5 skeletally mature mixed-breed dogs (weighing 19 to 30 kg) following euthanasia by IV administration of an overdose of pentobarbital. Specimens were disarticulated at the glenohumeral joint. Radiography was performed on each elbow joint and specimens were discarded if there was any evidence of osteoarthritis. Specimens were stored at –20 C and thawed to room temperature the day prior to testing. Physiologic saline (0.9% NaCl) solution was applied to soft tissues during testing to keep them moist.

Model—Soft tissues including skin, fascia, muscle, and neurovascular structures proximal to the elbow joint were removed, except for collateral ligaments and origins of the antebrachial muscles. The origin of the extensor carpi radialis muscle was dissected from the humerus, reflected distally, and partially excised by performing a myectomy proximal to the radial head. A transverse 4.0-mm transcondylar humeral bone tunnel was drilled. Medial and lateral epicondylar osteotomies were created, using an oscillating bone saw, around the drilled bone tunnel. Care was taken to ensure that articular cartilage was not damaged during the osteotomies. The epicondyles could be reflected distally, which preserved the integrity of the antebrachial myotendinous units and collateral ligaments (**Fig 1**). The epicondyles could be relocated anatomically and rigidly fixed by placement of a 3.8-mm transcondylar bolt and wing nut. Remnants of joint capsule and pericapsular fat were removed while preserving the annular ligament cranially and the distal half of the anconeus laterally.

The triceps brachii myotendinous unit was simulated by attaching a minimally distensable device from the proximal humeral metaphysis to the proximal aspect of the olecranon (**Fig 2**). Wire aircraft cable (84 kg test) was passed through two 6-mm humeral metaphyseal bone tunnels lined by metal rivets to prevent the wire cable from cutting through the bone. Cable was passed through 1 end of a turnbuckle and rigidly held to itself with a cable clamp. A 6-hole 2.7-mm veterinary reconstruction plate[a] was applied to the caudal aspect of the proximal ulnar shaft, using self-tapping 2.7 mm bicortical screws.[b] Screws that penetrated the transcortex and contacted the radius were removed or replaced. The proximal hole was left open and protruded above the olecranon. The hooked end of the turnbuckle was passed through the open screw hole of the plate. Adjustment of the turnbuckle allowed control over the length of the triceps mechanism and alteration of the angle at the elbow joint.

An external fixation apparatus was applied to each specimen to ensure repeatability of photographic positioning. Two half pins[c] were placed from the lateral aspect of the ante-

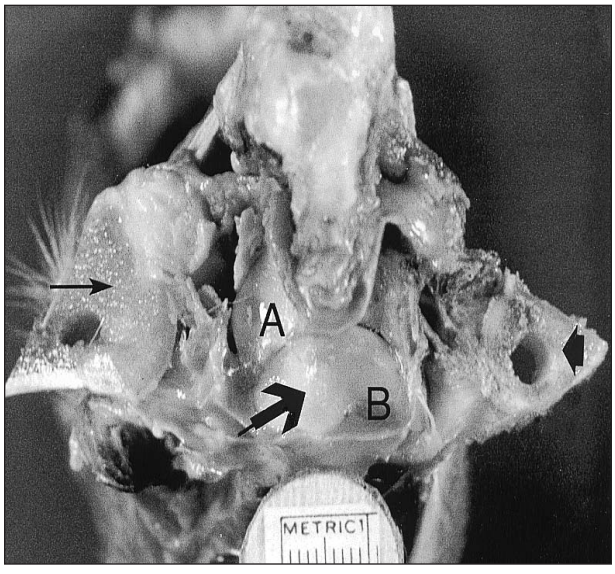

Figure 1—Photograph of disarticulated forelimb of a dog with joint cast in situ. Notice the medial (arrow) and lateral (arrowhead) epicondylar osteotomy sites and contact area (large arrow) on the proximal radial articular surface. A = Ulna. B = Radius.

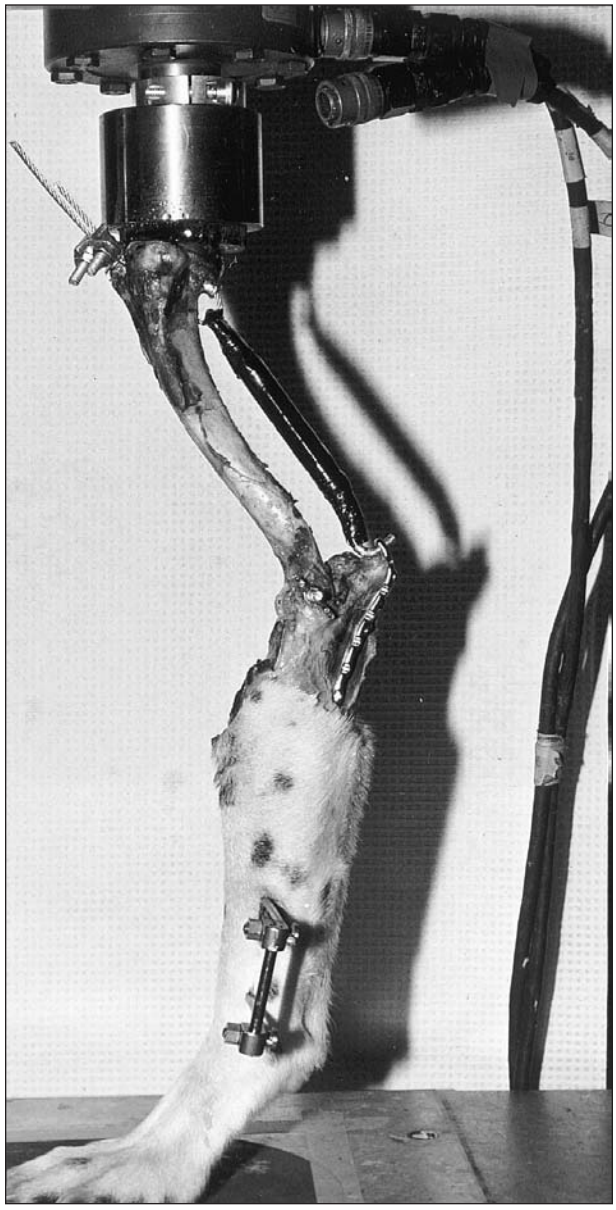

Figure 2—Photograph of articulated forelimb of a dog within the material testing system under an axial compressive load. The triceps brachii myotendinous unit was simulated by attaching an adjustable turnbuckle from the proximal humeral metaphysis to a contoured bone plate attached to the olecranon.

brachium into the distal radius parallel to the axis of the transcondylar bolt. One pin was placed at the level of the styloid process of the ulna and the other was placed 5 cm proximally in the radial diaphysis. External fixation clamps[d] and a connecting bar[e] were secured to the pins 3 cm lateral to the skin surface (Fig 2).

A 10-cm diameter circle of sandpaper was affixed to the platform of a **material testing system**[vi] **(MTS)** to minimize translation of the metacarpal and digital pads during loading. A concave rubber pad was attached to the load cell of the MTS to accept the convex shape of the humeral head. Each specimen was positioned within the MTS with the humeral head in the center of the load cell and the paw placed vertically under the humeral head.

Each specimen was statically loaded once to 12.5 **Newtons per kilogram of body weight (N/kg)** in the MTS to ensure that any slack in the cable attaching the turnbuckle to the humerus was eliminated. Turnbuckles were then adjusted for each specimen prior to casting to achieve an elbow flexion angle of approximately 135° based on the angle of the elbow joint during the midstance phase of the gait cycle.[17,18] Elbow joint angles were measured between the greater tubercle of the humerus, the center of the transcondylar bolt, and the medial styloid process of the radius.

Testing protocol—For each joint cast, 15 ml of viscous phase PMMA was applied to the combined radioulnar articular surface, with the humerus disarticulated from the elbow joint. The joint was then re-articulated and the epicondyles were repositioned anatomically and immobilized relative to the humeral diaphysis by insertion of the transcondylar bolt and hand tightening of the wing nut. The turnbuckle hook was then placed through the open hole of the ulnar plate. Care was taken to avoid inadvertent compression of the joint surfaces prior to placing specimens in the MTS. Specimens were axially compressed at a rate of 200 N/s until desired load was achieved. This load was maintained statically until the PMMA had cured. Elbow flexion angle was monitored during the entire period of loading to ensure maintenance of the angle between 130° and 140°. The load was then removed, and the elbow joint was disarticulated by unhooking the turnbuckle from the ulnar plate and removing the transepicondylar bolt and wing nut.

Phase I—Casting was performed on bilateral elbow joints of 1 dog under an axial load of 10.0 N/kg. Six casts of the right elbow joint were performed, followed by 6 casts of the left elbow joint.

Phase II—A series of 5 casts from the left forelimbs of 4 different dogs were made. For each specimen, axial load was progressively increased from an initial load of 2.5 N/kg to 12.5 N/kg in 2.5 N/kg increments. A joint cast was made at each different load for each specimen tested. The range of axial loads selected was based on the peak vertical ground reaction forces of dogs during walking (5 to 7.5 N/kg) and trotting (10 to 12.5 N/kg).[19-21]

Data collection—Five standardized photographic views of each cast were taken with an in-frame metric scale **(Fig 3-7)**. Repeatable orientation of the specimen was achieved by securing the external fixator connecting bar in 1 of 5 clamps attached to a supporting apparatus. After imaging of casts was complete, water-soluble paint was sprayed onto the proximal ends of the radius and ulna to completely cover the casts and any exposed cartilage surfaces. Paint was allowed to dry and thumb forceps were used to remove the casts. Care was taken to avoid removing paint on exposed cartilage during cast removal. The combined radioulnar articular surfaces were photographed, using identical views as described. Paint was removed from cartilage surfaces with a saline soaked sponge.

Areas of cartilage contact were measured on both the cast and painted images. Areas of radial articular surface in contact were measured from a view taken perpendicular to the radial head (radial view), taking care to avoid superimposition of the anconeus (Fig 1, 4). Areas of distal ulnar articular surface were measured on 2 photographic views. The first view was perpendicular to the medial coronoid process (coronoid view; Fig 5). The second view was taken from the medial aspect of the limb, parallel to the axis of rotation of the humeroulnar joint, centering the camera over the middle of the trochlear notch (medial ulnar view; Fig 6). Areas of proximal ulnar articular surface in contact were measured from 2 views. The first view was taken from the proximal aspect of the trochlear notch of the ulna from the cranial aspect (cranial ulnar view; Fig 3). The camera was positioned along the sagittal plane of elbow flexion. The second view was taken from the lateral aspect of the ulna, parallel to the

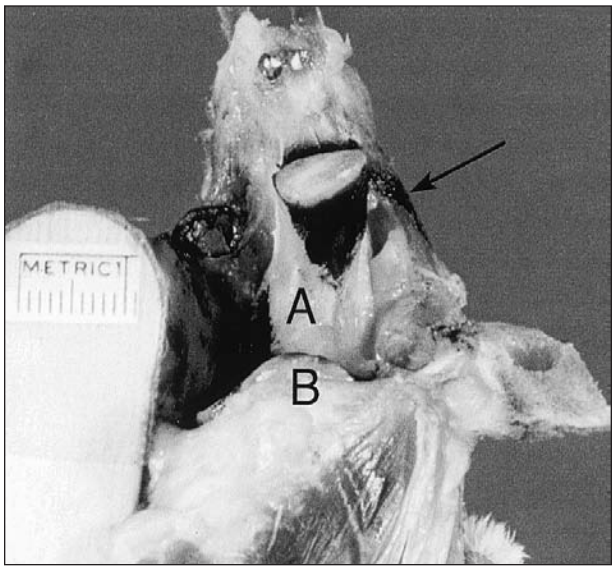

Figure 3—Photographic view of the cranial aspect of the ulna in the elbow joint (cranial ulnar view). Notice black paint on proximal contact area (arrow). A = Ulna. B = Radius.

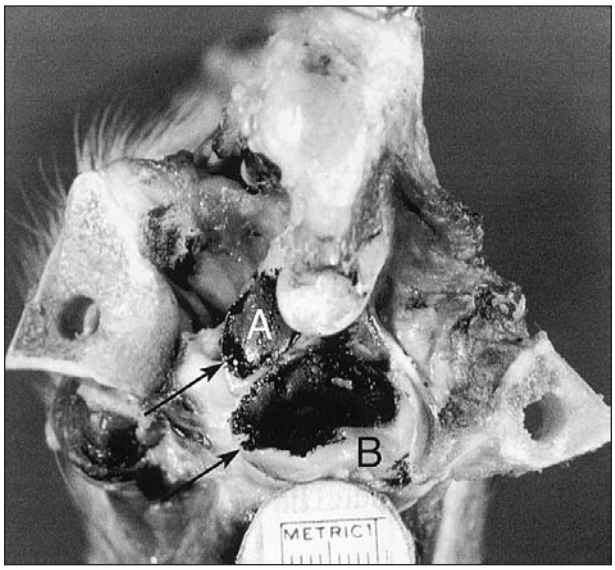

Figure 4—Photographic view of the radial articular surface of the elbow joint (radial view). Notice black paint on the radial and distal ulnar contact areas (arrows). A = Ulna. B = Radius.

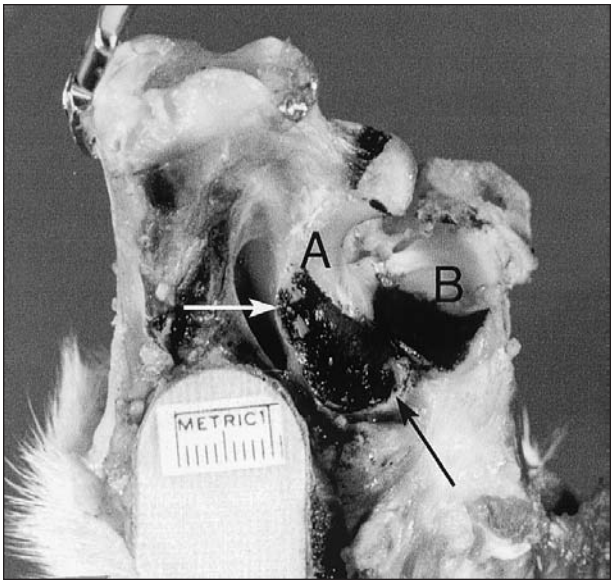

Figure 5—Photographic view of the medial coronoid process of the elbow joint (coronoid view). Notice black paint on the distal ulnar contact area (arrows). A = Ulna. B = Radius.

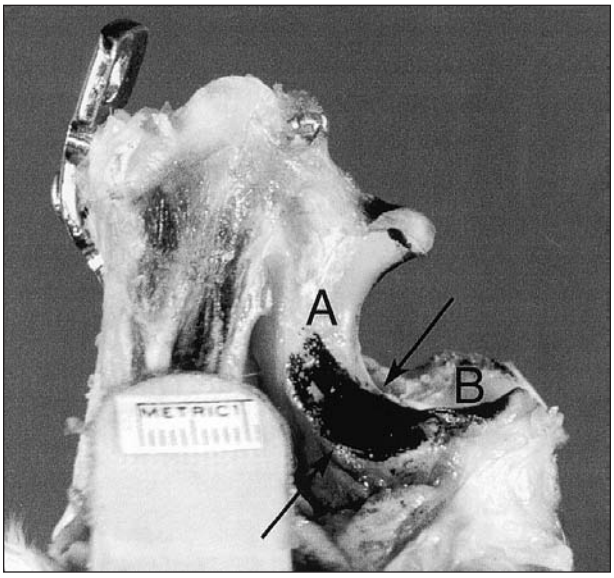

Figure 6—Photographic view of the medial aspect of the ulna of the elbow joint (medial ulnar view). Notice black paint on distal ulnar contact area (arrows). A = Ulna. B = Radius.

axis of rotation of the humeroulnar joint, centering the camera over the middle of the trochlear notch (lateral ulnar view; Fig 7).

Color 35-mm transparencies[g] were digitized with a high resolution scanner[h] and transferred to a personal computer.[i] Contact areas from both cast and paint images were measured by use of image analysis software.[j] To calculate contact areas from cast images, radial or ulnar cartilage surfaces not covered by casting agent were considered to be contact areas. Conversely, when considering painted images, cartilage surfaces covered in paint were considered to be contact areas. Contact areas were defined for each photographic view and represented components of the combined cartilage surfaces of the radius or ulna that contacted the distal articular surface of the humerus. For each view, measured contact areas were divided by the respective contact area to yield relative

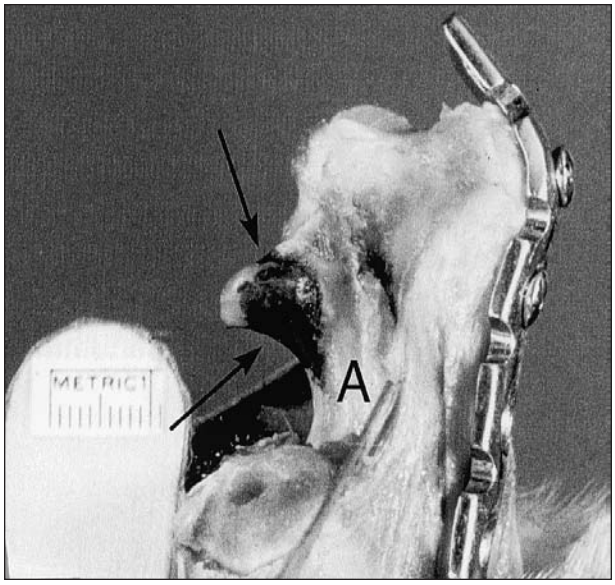

Figure 7—Photographic view of the lateral aspect of the ulna of the elbow joint (lateral ulnar view). Notice black paint on proximal ulnar contact area (arrows). A = Ulna. B = Radius.

contact areas. Specific nonoverlapping regions of each articular surface were evaluated from each view to avoid a false increase in contact area and relative contact area.

Statistical analyses—Repeatability of casting and painting methods was assessed by calculation of the coefficient of variation on up to 8 replicates from a single dog. Within-dog left versus right differences were evaluated by use of Student *t*-test. Two within-factor repeated-measures ANOVA were used to evaluate effects of loading on relative contact area from paint and cast images, and whether any such effect differed between the 5 photographic views. Values of $P < 0.05$ were considered significant.

Results

Quality of joint casts varied between trials and improved over time concomitant with operator experience. Casts of poor quality were discarded and the previous loading condition repeated. Approximately half of the casts fractured and dislodged during humeral disarticulation. Dislodged cast fragments were manually replaced to their appropriate anatomic location. Loss of contact area data, when photographing joint casts in situ, was observed in 19.4% (33/170) of images, primarily in phase I of the study. During the initial phase I trials, excessive casting agent often leaked out of the contact region, where it hardened and subsequently obscured the photographic views. This affected primarily the coronoid, medial, and lateral views, but had little effect on the radial and anconeal views. The loss of data did not affect the statistical determination of repeatability of phase I.

Contact areas were easily identified by the lack of casting agent and exposure of underlying articular cartilage. These areas were oval-shaped, with smooth, well-demarcated edges (Fig 1). Several casts had poor demarcation at the transition zone between contact and noncontact areas where thin, transparent casting agent was seen. The circumferential contour of these casts was irregular. There appeared to be an association

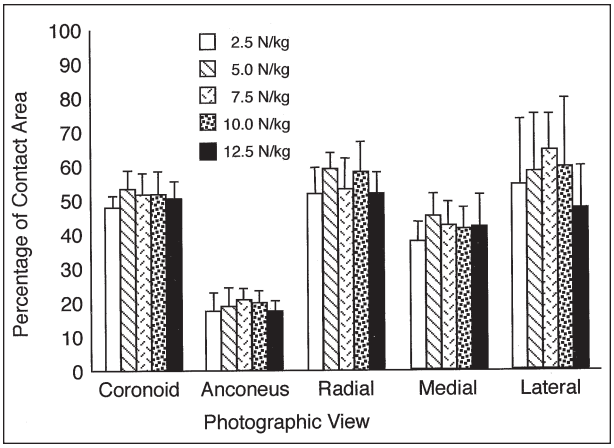

Figure 8—Mean percentage (± SD) of relative cartilage contact area for 5 axial loads on the elbow joint in dogs. Percentages were determined by calculating contact area from 5 photographic views of curved surfaces of the joint, following application of polymethyl methacrylate to joint surfaces. N/kg = Newtons per kilogram of body weight.

between the increased time interval between PMMA mixing and specimen loading, and a poor quality cast with irregular edges at the periphery of the contact areas.

All casts revealed 3 discrete contact areas. A radial contact area was located on the caudomedial aspect of the proximal radial articular surface, with its longest dimension oriented mediolaterally (Fig 1, 4). A second contact area was located on the medial aspect of the distal articular surface of the trochlear notch, and extended to the lateral edge of the medial coronoid process (Fig 5, 6). A third contact area was located on the craniolateral surface of the proximal trochlear notch (Fig 3, 7).

Phase I—Coefficients of variation for the relative contact areas, calculated for each of the 5 views, remained < 20%, documenting repeatability of the casting technique in the elbow joint. Significant differences in relative contact areas between left and right sides from the same cadaver were not detected, nor were significant differences detected between the relative contact areas that were calculated from the cast and painted images. No specific advantages were recognized in feasibility or accuracy between digital analysis of casted joint surfaces and painted joint surfaces.

Phase II—For both casted and painted images, there were no consistent dose-responses observed with increased loading (**Fig 8**). Significant overall load effects on relative contact area for casted and painted regions were not detected ($P = 0.19$ and 0.11, respectively). In 95% (19/20) of trials in phase II of the study, the coronoid contact area was continuous with the radial contact area at the lateral aspect of the medial coronoid process (Fig 1, 4, 5). This combined contact area was several millimeters wide at the lateral edge of the medial coronoid process.

Discussion

Results of this study suggested that during the stance phase of the gait cycle in dogs, when axial load on the elbow joint is < 12.5 N/kg, there are 3 distinct areas of the combined radioulnar articular surface that are in contact with the humeral trochlea and capitulum. Specific areas of articular contact were identified on the radius, the craniolateral aspect of the anconeus, and the medial coronoid process. The medial coronoid and radial contact areas were continuous across the radioulnar articulation. Lack of articular contact was identified on the medial aspect of the anconeus and the central trochlear notch. Significant overall effects of axial load on contact area or location were not identified. The findings of this study support the hypothesis that physiologic concave incongruity does exist between weight-bearing surfaces of the humerus and ulna. Concave incongruity may be defined as a difference in shape or radius of a diarthrodial joint, resulting in peripheral articular contact and increased central joint space.[9] In the elbow joint, this is likely a result of the radius of the concave surface being smaller than the radius of the convex surface. Geometric incongruity in normal joints serves to optimize stress distribution during loading.[9,15,22] Eckstein[9] demonstrated that the trochlear notch of the ulna in humans is deeper than necessary for an exact fit with the trochlea of the humerus. The resulting concave incongruity produces bicentric transmission of forces at low loads.[9] Concave incongruity disappears as loading increases, because of the deformability of cartilage and subchondral bone and eventually during maximal loading, and a state of congruence is reached in which the load is transmitted more homogeneously.[9] Finite element modeling, comparing stress distribution in congruous and incongruous joints, has supported the concept that deeper sockets lead to bicentric force transmission, which lowers peak stresses within joints under high loading conditions.[9,15] It has been suggested that physiologic incongruity leads to a more even distribution of stress, provides intermittent stimulation of cartilaginous tissue, and has beneficial effects on metabolism, nutrition, and lubrication of articular cartilage during cyclic loading.[15] In phase II of our study, convergence of the 2 ulnar contact areas or enlargement of the relative contact areas for each view was not seen under increasing loading conditions. Magnitude of axial loads applied to the limbs in this study may have been insufficient to demonstrate a load-dependent change in contact patterns. Alternatively, convergence of contact areas as seen in the elbow joint in humans may not be present in the elbow joint in dogs because of the extended position of the joint during normal ambulation.

Casting techniques are sensitive to step defects in articular geometry; continuity of contact areas across an articulation strongly suggests that adjacent articular surfaces are level.[2,6,14] Continuity of coronoid and radial contact areas across the lateral edge of the medial coronoid process in all but 1 of the casts in phase II of our study suggested that there is no step between the coronoid process and the radius during the stance phase of the gait cycle. This finding supports the theory that asynchronous growth between the radius and ulna (creating a step at the medial aspect of the radioulnar articulation) would contribute to abnormal stress distribution and potential mechanical overloading of the medial coronoid process.

Accurate in vitro determination of joint contact areas is dependent on simulating in vivo conditions as closely as possible.[3] This includes preservation of periarticular connective tissue structures and application of physiologic loading conditions.[3] Both collateral ligaments were maintained in our model by creating osteotomies that could be anatomically repositioned and compressed to the humeral condyle, minimizing movement at the osteotomy interfaces. Studies in human cadavers have further revealed that immobilization of adjacent joints affects contact patterns in the joints of interest.[12] Physiologically relevant in vitro models must therefore preserve adjacent articulations. In our study, this was achieved by preserving the carpus and paw to allow axial forces to be transmitted anatomically through the digital and metacarpal pads and to allow carpal and digital flexor myotendinous units to resist carpal and digital hyperextension, respectively.

The only myotendinous unit spanning the elbow joint to be simulated in this model was the triceps brachii. Although tensile forces in the triceps brachii myotendinous unit during weight-bearing are unknown, the minimally distensable triceps model was based on the assumption that during the midstance phase of the gait cycle, when the angle of the elbow is fixed, the movement created by vertical ground reaction forces and gravity are balanced by the movement created by active muscle contraction of the triceps brachii unit.

Studies comparing the accuracy of cartilage staining, casting, and pressure sensitive film in the determination of joint contact areas have concluded that although some techniques consistently under- or overestimate the perceived contact, all techniques are highly repeatable and yield comparable data.[1-3,5,13,23,24] Use of pressure sensitive film has the advantage of quantitating force transmission across joints; however, it is difficult to use between highly curved surfaces. Cartilage staining involves injection of colored dyes into joints; dyes help to identify noncontact surfaces, leaving the contact areas exposed. Casting techniques involve the squeeze-film effect, where liquid phase casting agents are driven out of the region of contact as the 2 articular surfaces are compressed together. Casting agents are never entirely squeezed out of contact areas because of their increased viscosity, and thus actual contact areas are often underestimated or there may be a failure to detect contact in some regions of a joint.[1] Silicone rubber used as a casting agent has the advantage that it remains flexible, permitting cast retrieval after each trial.[2] These casts can later be applied to articular surfaces, allowing determination of contact areas on more than 1 surface.[2] In addition, these casts can be removed and flattened for measurement of contact area. A solid casting agent was used in our study on the basis of our assessment that solid casts have greater repeatability. The inability to flatten solid casts necessitated photographing them on the joint surface. Calculation of area from photographic views of curved surfaces may result in some distortion of actual area because of parallax. However, we believe this had little effect on the results of this study because the relatively flat areas were isolated to each view, and applied to repeatability of photographic positioning.

There was a learning curve with the use of PMMA for contact area determination in this study. Delays between application of liquid phase PMMA to the articular surfaces and loading in the MTS appeared to correlate with a cast having reduced or no contact areas. Intuitively, this developed because the casting agent was too viscous when load was applied, preventing the true contact areas from coming into apposition. This problem was minimized by applying PMMA when it was viscous rather than doughy, and minimizing the lag time from placement of the limb in the MTS to load application by programming the MTS control unit to load at a rate of 200 N/s. Of higher concern was the fact that some peripheral areas that appeared to be consistently devoid of casting material but were assumed to be true contact areas were sometimes covered by a thin film of PMMA. These thin films of PMMA had highly irregular edges and varied considerably in size. These areas were regarded as artifact rather than noncontact areas because of their variability in size and distribution, and because they were not consistently present in identical specimens under fixed loading conditions. Areas covered by these thin PMMA layers were considered to contribute to contact areas when data was collected. Fracture of casts during disarticulation was common if the periphery of the cast was thin or regions of the cast were not connected by sufficient bulk. This was addressed by recording the location of areas that commonly fragmented, and applying more PMMA to these areas. Despite these technical difficulties, the technique of PMMA joint casting provided a high degree of repeatability for determination of general regions of joint surface contact in the elbow. Although the small sample size limited the statistical power of both phases of this study, the magnitude of differences in relative contact areas observed were not compelling enough to warrant investigation of further specimens.

To our knowledge, areas of cartilage contact in the elbow joint of dogs have not been reported. Knowledge of elbow joint contact mechanics may play a major role in determining the underlying pathophysiologic characteristics of diseases that lead to osteoarthritis. Baseline information will allow for comparison of surface interactions in instances of dysplasia of the elbow joint, as well as for evaluation of the effects of corrective osteotomies to improve abnormal contact mechanics.

[a]8-hole, 64-mm, 2.7-mm Reconstruction plate, Synthes, Monument, Colo.
[b]2.7-mm self-tapping cortical orthopedic screws, Synthes, Monumet, Colo.
[c]Medium 1/8" shank, 5/32" thread interface fixation half pin, IMEX Vet Inc, Longview, Tex.
[d]Medium external fixation clamp, IMEX Vet Inc, Longview, Tex.
[e]Medium connecting bar, IMEX Vet Inc, Longview, Tex.
[f]Teststar Materials Test System, MTS systems corporation, Eden Prairie, Minn.
[g]Ektachrome, Kodak, Rochester, NY.
[h]RFS 3570 Film Scanner, Kodak, Rochester, NY.
[i]Apple Power McIntosh 8100, Apple Computer Inc, Coopertino, Calif.
[j]NIH Image 1.60, National Institutes of Health, Bethesda, Md.

References

1. Ateshian GA, Kwak SD, Soslowsky LJ. A stereophotogram-

metric method for determining *in situ* contact areas in diarthrodial joint and a comparison with other methods. *J Biomech* 1994; 27:111–124.

2. Stormont TJ, An K-N, Morrey BF, et al. Elbow joint contact study; comparison of techniques. *J Biomech* 1998;18:329–336.

3. Olson SA, Bay BK, Hamel A. Biomechanics of the hip joint and the effects of fracture of the acetabulum. *Clin Orthop* 1997;339: 92–104.

4. Ronsky JL, Herzog W, Brown TD. In vivo quantification of the cat patellofemoral joint contact areas and stresses. *J Biomech* 1995;28:977–983.

5. Driscoll HL, Christensen JC, Tencer AF. Contact characteristics of the ankle. Part I: the normal joint. *J Am Podiatr Med Assoc* 1994;84:491–498.

6. Goel VK, Singh D, Bijlani V. Contact areas in human elbow joints. *J Biomech Eng* 1982;104:169–175.

7. Dejardin LM, Perry RL, Arnoczky SP. The effect of triple pelvic osteotomy on the articular contact area of the hip joint in dysplastic dogs: an in vitro experimental study. *Vet Surg* 1998; 27:194–202.

8. Simon WH, Friedenberg S, Richardson S. A correlation of joint congruence and thickness of articular cartilage in dogs. *J Bone Joint Surg* 1973;55A:1614–1621.

9. Eckstein F, Lohe F, Muller-Gerbl M. Stress distribution in the trochlea notch. A model of bicentric load transmission through joints. *J Bone Joint Surg* 1994;76B:647–653.

10. Hak DJ, Hammel AJ, Bay BK. Consequences of transverse acetabular frature malreduction on load transmission across the hip joint. *J Orthop Trauma* 1998;12:90–100.

11. Garrett JC, Kress KJ, Mundaro M. Osteochonditis dessicans of the lateral femoral condyle in the adult. *J Arthritis Rel Surg* 1992;8: 474–481.

12. Wang CL, Cheng C, Chen CW. Contact areas and pressure distribution in the subtalar jont. *J Biomech* 1995;28:269–279.

13. Viegas SF, Patterson RM. Load mechanics of the wrist. *Hand Clin* 1997;13:109–128.

14. Mow VC, Ateshian GA, Spilker RL. Biomechanics of diarthrodial joints: a review of twenty years of progress. *J Biomech Eng* 1993;15:460–467.

15. Eckstein F, Merz B, Muller-Gerbl M. Morphomechanics of the humero-ulnar joint: concave incongruity determines the distribution of load and subchondral mineralisation. *Anat Rec* 1995;243: 327–335.

16. Eckstein F, Lohe F, Schulte E. Physiological incongruity of the humero-ulnar joint: a functional principle of optimized stress distribution acting upon the articulating surface? *Anat Embryol* 1993;188:449–455.

17. DeCamp CE, Soutas-Little RW, Hauptman J. Kinematic gait analysis of the trot in healthy greyhounds. *Am J Vet Res* 1993;54: 627–634.

18. Allen K, DeCamp CE, Braden TD. Kinematic gait analysis of the trot in healthy mixed breed dogs. *Vet Comp Orthop Trauma* 1994;7:148–153.

19. Riggs CM, DeCamp CE, Soutas-Little RW, et al. Effects of subject velocity on force plate-measured ground reaction forces in healthy greyhounds at the trot. *Am J Vet Res* 1993;54:1523–1526.

20. Anderson MA, Mann FA. Force plate analysis: a noninvasive tool for gait evaluation. *Compend Contin Educ Pract Vet* 1994; 16:857–866.

21. Rumph PF, Lander JE, Kincaid SA, et al. Ground reaction force profiles from force platform gait analyses of clinically normal mesomorphic dogs at the trot. *Am J Vet Res* 1994;55:756–761.

22. Eckstein F, Lohe F, Schulte E, et al. Physiological incongruity of the humero-ulnar joint: a functional principle of optimized stress distribution acting upon articulating surfaces. *Anat Embryol* 1993;188:449–455.

23. Cullen JP, Parentis MA, Chincilli VM. Simulated bennett fracture treated with closed reduction and percutaneous pinning. *J Bone Joint Surg* 1997;79-A:413–420.

24. Pereira DS, Koval KJ, Resnick RB. Tibiotalar contact area and pressure distribution: the effect of mortise widening and syndesmosis fixation. *Foot Ankle Int* 1996;17:269–274.

25. Olson SA, Bay BK, Hamel A. Biomechanics of the hip joint and the effects of fracture of the actetabulum. *Clin Orthop* 1997; 339:92–104.

26. Yanoff SR, Hulse DA, Hogan HA, et al. Measurements of vertical graound reaction forces in jumping dogs. *Vet Comp Orthop Trauma* 1992;5:44–50.